Direct observation of symmetry-specific precession in a ferrimagnet

P. Warnicke,[1,*] E. Stavitski,[1] J.-S. Lee,[1,†] A. Yang,[2,‡] Z. Chen,[2,‡] X. Zuo,[2,§] S. Zohar,[3,‖] W. E. Bailey,[3] V. G. Harris,[2] and D. A. Arena[1,¶]

[1]*Photon Sciences Directorate, Brookhaven National Laboratory, Upton, New York 11973, USA*

[2]*Department of Electrical and Computer Engineering, Northeastern University, Boston, Massachusetts 02115, USA*

[3]*Materials Science Program, Department of Applied Physics, Columbia University, New York, New York 10027, USA*

(Received 17 March 2014; published 1 September 2015)

Here we demonstrate an experimental observation of GHz-scale spin dynamics resolved to sublattice octahedral (O_h) tetrahedral (T_d) sites in a spinel ferrimagnet, in this case a Mn-ferrite thin film. X-ray absorption spectroscopy (XAS) and x-ray magnetic circular dichroism (XMCD) are used, in combination with multiplet calculations, to uniquely identify the spectral signature from Mn^{2+} and $Fe^{2+,3+}$ on O_h and T_d lattice sites. With the sample under *rf* excitation, the spin alignment of the sublattices is tracked with time-resolved XMCD (TR-XMCD). The spin alignment of the sublattices is mostly antiferromagnetic. The phase difference between the O_h Fe^{2+} [O_h Fe^{3+}] and T_d Mn^{2+} sites is $181.2 \pm 3.8^\circ$ [$183.3^\circ \pm 3.7^\circ$] at 150 K and $186.6 \pm 2.2^\circ$ [$182.0^\circ \pm 2.2^\circ$] at 300 K. Such direct measurement of the dynamic coupling, exchange stiffness, and damping enabled by TR-XMCD across sublattices will be essential for optimizing the development of future-generation microwave devices.

DOI: 10.1103/PhysRevB.92.104402 PACS number(s): 75.50.Gg, 75.47.Lx, 78.47.D−, 78.70.Dm

I. INTRODUCTION

Magnetic oxides such as ferrites have wide ranging applications and in thin film form the unique properties of ferrites are increasingly applied to new uses such as integrated microwave devices [1] and spin filters [2–5]; most of these new applications require superior microwave performance (e.g., low resonance linewidth). Spinel ferrites, with a chemical formula of AB_2O_4, are a common choice for high-frequency applications [6]. However, a challenge in obtaining appropriate high-frequency characteristics is controlling the distribution across and interactions between metal cations in the octahedral (O_h) and tetrahedral (T_d) sub-lattices in the spinel structure. Hence it is important to examine the dynamic coupling and other interactions of the different sublattices at time scales relevant to high-frequency (GHz-level) applications.

In microwave devices, a planar geometry is desirable for compatibility with integrated circuit (IC) design, leading to intensive recent efforts on developing ferrite films with specific magnetic and microwave properties [7]. In devices such as circulators, isolators, and phase shifters, the off-resonance microwave properties of ferrites often determine the output characteristics such as insertion loss and nonreciprocal attenuation. For model systems, studies of epitaxial ferrite thin films grown on lattice matched substrates reveal details on development of net magnetic moment, strain effects, crystalline anisotropy, and relationships between extrinsic and intrinsic ferromagnetic resonance (FMR) losses [8]. Polycrystalline films are more compatible with IC production systems and offer additional mechanisms for tuning properties via control of crystallite size and magnetic coupling across crystallites [7], although the variation of crystalline anisotropy axes in polycrystalline films can lead to broader FMR linewidth. Also, polycrystalline films can be grown on amorphous substrates, which is advantageous for soft x-ray magnetic spectroscopy of ferrite films.

X-ray absorption spectroscopy (XAS) in the soft x-ray spectral range is a technique that is well-suited for examining issues such as cation valence and crystal field symmetry and strength [9]. In addition, x-ray magnetic circular dichroism (XMCD) can reveal details of magnetic alignment between different cations [10–15].

By applying XAS and XMCD we examine the role of sample processing conditions on the cation distribution and verify in our films the net alignment of Mn and Fe cations. More importantly, we use a combination of time-resolved XMCD (TR-XMCD) and microwave excitation to examine the precessional motion of cations resolved to specific T_d or O_h sublattices. By stroboscopically sampling the precessional orbit of the cations, we present measurements of the phase relationship of the cations on the O_h and T_d sites under driven precession, opening a direct path to future tests of lagged response models of intrinsic loss mechanisms in mixed valence magnetic oxides [16].

In the full spinel crystal structure, A^{2+} cations occupy T_d sites and B^{3+} cations reside on O_h sites while in an inverse spinel, the B^{3+} cations are divided equally between the O_h and T_d sites, and all of A^{2+} cations occupy O_h sites [see Fig. 1(a)]. Mn ferrite is a partial inverse spinel, where the electronic similarity of manganous (Mn^{2+}) and ferric (Fe^{3+}) cations leads to a redistribution across the T_d and O_h sites; on average in bulk systems, around 20% of the Mn^{2+} cations reside on the O_h sites [17]. The degree of inversion determines the net magnetic moment in Mn ferrites (the T_d and O_h sites

*Swiss Light Source, Paul Scherrer Institut, 5232 Villigen, Switzerland.

†SSRL, SLAC National Accelerator Lab, Menlo Park, CA 94025, USA.

‡HGST, a Western Digital Company, San Jose, CA 95135, USA.

§College of Information Technical Science, Nankai University, Tianjin 300071, China.

‖Advanced Photon Source, Argonne National Lab, Argonne, IL 60439, USA.

¶Corresponding author: darena@usf.edu; current address: Department of Physics, University of South Florida, Tampa, FL 33620-7100, USA.

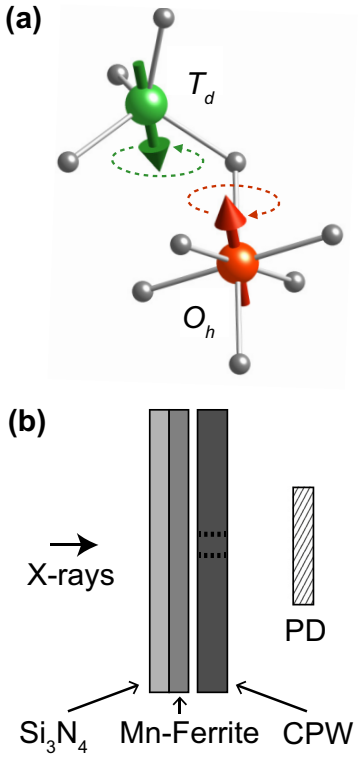

FIG. 1. (Color online) (a) Illustrative closeup of a portion of the spinel crystal structure highlighting cations in an octahedral (red) and tetrahedral (green) crystal field. The antiferromagnetic coupling between adjacent cation spins (arrows) are mediated through oxygen anions (gray). Subjected to a microwave field, the spins in the lattice are excited to precession (indicated by dashed lines). (b) Schematic of the experimental design with the Mn ferrite deposited on a semitransparent silicon nitride membrane positioned close to a coplanar waveguide (CPW). The ferrite is measured in transmission mode by synchrotron x rays which are phase-locked to the microwave excitation field generated by the CPW. Transmitted x rays are detected by a photodiode (PD).

are antiferromagnetically coupled), and can also can affect the uniaxial anisotropy [18].

II. SAMPLES AND METHODS

Here, we look at Mn-ferrite films grown on amorphous silicon nitride (Si_3N_4). These thin films were grown under nonequilibrium conditions by pulsed laser deposition using dual targets and alternating target laser ablation deposition (ATLAD) [19]. To prepare the laser ablation targets, 20 grams of starting powders (Fe_2O_3 or Mn_3O_4) were ball milled for 2 h; the mixing was performed in 60 ml alcohol with the weight ratio powders:ball = 1:5. After the ball mill process, the slurry is dried, pressed into a disk and then calcined at 900 °C for 2 h in air. The heating and the cooling rate were both 5 °C/min. The calcined samples were crushed and ball milled for an additional 6–8 h, and the grinding performed in 40 ml alcohol with the weight ratio powders:ball = 1:10. After this step, the average grain size of the ferrite powder was about 1–2 μm. The ferrite powders were granulated with 10 wt. % polyvinyl alcohol (PVA) and classified for use by mechanical sieving under 400 μm. Finally, the powders were pressed into disks of 25 mm diameter. Disk samples were sintered in air at 1280–1320 °C for 4 h, at 900 °C, while the oxygen concentration was lowered from that of air to 5–10 vol % of oxygen, then cooled in nitrogen atmosphere by 2 °C/min. The films grown via ATLAD from these targets had a nominal thickness of 50 nm, and were deposited onto silicon nitride membranes using a growth temperature of 750 or 810 °C and an O_2 pressure of 2 or 10 mTorr (see Table I). Under these processing conditions, the 750 °C, 2 mTorr sample grown on amorphous silicon nitride exhibited a saturation magnetization (M_s) and M vs T behavior very similar to Mn ferrite films grown by ATLAD on single crystal MgO substrates under similar processing conditions [20,21].

TABLE I. Samples and processing conditions. The two rightmost columns contain the relative amounts of Mn and Fe cations.

Sample	T_{growth} (°C)	P_{growth} (mTorr)	Mn^{2+}/ Mn^{3+}	Fe^{2+}/ Fe^{3+}
I	750	10	0.72 : 0.28	0.17 : 0.83
II	750	2	0.98 : 0.02	0.19 : 0.81
III	810	10	0.93 : 0.07	0.19 : 0.81
IV	810	2	1 : 0	0.22 : 0.78

Both XAS and XMCD were measured in transmission mode, where the transmitted x-ray intensity was monitored as a function of photon energy [see Fig. 1(b)]. Measurements of the precessional motion were carried out at beamline 4-ID-C of the Advance Photon Source (APS) at Argonne National Laboratory. Alternating magnetic fields, harmonically generated and phase-locked to the electron bunches of the synchrotron, were applied to the sample via a coplanar waveguide to excite precession of the magnetic moments. Due to shape anisotropy of the thin film samples the precessional orbit of the magnetization vector is strongly elliptical with an in-plane long axis. As the XMCD signal is proportional to the projection of the magnetization along the light propagation vector the sample was rotated 30° away from normal incidence to increase the signal-to-background level. Element- and time-resolved scans were generated by monitoring the XMCD intensity while varying the time delay between the bunches and the microwave excitation. More details on the XMCD + FMR apparatus are reported in [22]. The measurements were carried out at room temperature (RT) and at 150 K.

III. RESULTS

Static transmission XAS and XMCD spectra were obtained for Fe and Mn, respectively, by scanning the incident photon energy over the corresponding L edges. XAS (XMCD) spectra are presented as the average (difference) of individual spectra collected with the sample magnetization and photon helicity in aligned and antialigned configurations. Spectra for films prepared under different processing conditions are presented in Fig. 2. A linear background is subtracted from all experimental spectra and the L_3 peak height on both the XAS and XMCD data sets is normalized to unity to facilitate comparison.

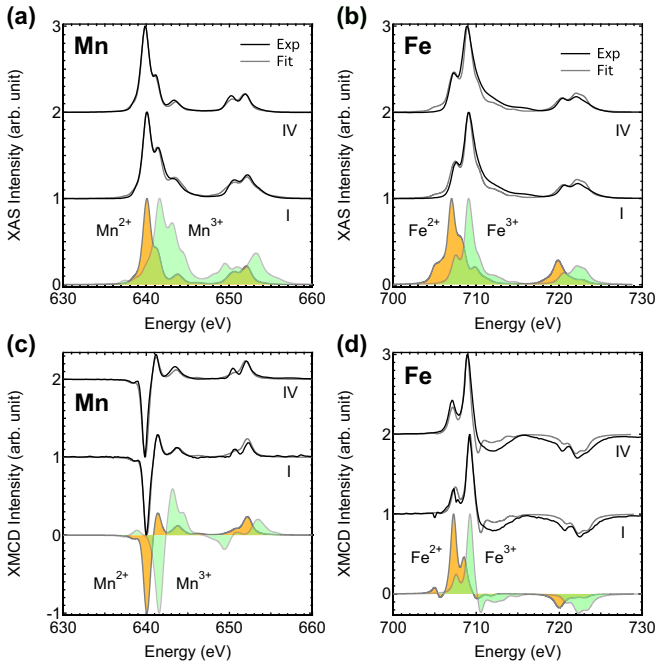

FIG. 2. (Color online) X-ray spectroscopy of Mn-ferrite films grown using different processing conditions according to Table I showing XAS (top row) and XMCD (bottom row) spectra for Mn (left column) and Fe (right column). Experimental data (black) are fitted (gray) for samples I and IV which exhibit the largest relative difference in cation composition. Calculated divalent (yellow) and trivalent (green) XAS and XMCD spectra for the cations are presented in the bottom of corresponding subfigure. The XMCD spectra are displayed in solid colors for visual clarity. Details on the fits are presented in the text.

To assess the distribution of cations with different oxidation state and site occupancy, we model the experimental XAS and XMCD spectra with multiplet calculations based on the method described by van der Laan and Thole [23] using CTM4XAS software [24,25]. The best fit to the experimental spectra were obtained with a crystal field parameter of $10D_q = 0.6$ and 1 eV for Mn^{2+} and Mn^{3+} respectively, close to those found for related systems [26] for Mn cations located in T_d symmetry. The Fe spectra were modeled assuming a combination of Fe^{3+} ($10D_q = 1.4$ eV) and Fe^{2+} ($10D_q = 1.2$ eV), both occupying O_h sites. The crystal field values are similar to those found in Fe_3O_4 [27] and manganese ferrites [28]. Hybridization between the d orbitals of the metal ions and p orbitals of oxygen in the lattice was taken into account indirectly by reducing Slater parameters to 80% of their atomic value [29]. The XMCD spectra were simulated by assuming a constant exchange field of 5 meV. Good fits to the experimental spectra were obtained (gray traces in Fig. 2), allowing us to determine the relative concentrations of divalent and trivalent cations. We also assign the main spectral features on the XMCD traces to cations residing either on T_d or O_h sites (see below).

The two rightmost columns in Table I summarize the relative concentrations of divalent and trivalent cations; the error of the relative intensities is estimated at about 10%. As can be seen in the table, the majority of the metal ions are the thermodynamically stable manganous (Mn^{2+}) and ferric (Fe^{3+}) cations. The fits to the Fe spectra indicate that the Fe oxidation state in these samples is relatively insensitive to processing conditions, although the presence of divalent Fe in the sample may indicate a small amount of oxygen deficiency in the films. The fits to the Mn spectra reveal a similar trend, with the exception of the sample prepared at 750 °C and 10 mTorr O_2; this sample has a significant contribution from Mn^{3+}, which is consistent with the observation that the Mn valence is more sensitive to sample processing conditions [20].

The XMCD spectra in Fig. 2 confirm that the Mn and Fe cations are antiferromagnetically aligned, consistent with the assumption of predominant T_d occupation for the Mn cations and O_h occupation for the Fe cations. The modeling of the XMCD spectra indicates that the main peaks in the L_3 edge XMCD spectra for Fe (707 eV and 709.5 eV) can be assigned primarily to Fe^{2+} and Fe^{3+}, respectively. Interestingly, the XMCD spectra for Mn are reproduced in the models assuming that only the Mn^{2+} cations contribute to the XMCD signal, suggesting that the Mn^{3+} cations do not have a net ferromagnetic alignment, possibly due to the localization of these ions in the near-surface layer, similar to the case of CrO_2 thin films [30]. Site inversion (transfer of a fraction of the Mn^{2+} cations from T_d to O_h sites, along with a concomitant shift of Fe cations to T_d sites) often occurs in Mn-ferrite samples [26,28,31]; however, the degree of inversion in Mn-ferrite samples (typically on the order of 20%) does not affect the assignment of the main features of the XMCD spectra to Mn^{2+} on T_d sites and $Fe^{2+,3+}$ cations on O_h sites. Note that the primary effect of inversion involving the divalent Mn and trivalent Fe cations (both with $3d^5$ orbital population) would be the reduction of the main XMCD signal for those cations without changing the energy of the peaks in the XMCD spectra.

Turning now to the TR-XMCD measurements, we first examine a Mn-ferrite sample prepared under similar growth conditions using static XAS and XMCD; results are presented in Figs. 3(a) and 3(b). Fits to the XAS scans indicate that, within the estimated error of the fits, the cation distribution is identical to sample I. As with the other samples, modeling of the XMCD spectra confirm the assignments of the XMCD peaks at 639.2 eV to Mn^{2+} cations on the T_d sites and the peaks at 707 eV and 709.5 eV to Fe^{2+} and Fe^{3+}, respectively, on the O_h coordinated sites.

Although the time-resolved technique described here allows for measurements at higher frequencies we choose to work at a relatively low excitation *rf* in order to maintain a large precession angle and hence a substantial XMCD signal [32]. Microwave excitations at a frequency of 2.1 GHz, phase locked with the x-ray bunch clock as described in [22], are applied to the sample via a coplanar waveguide while an orthogonal, in-plane 95 Oe bias field is applied. The *rf* excitation produces precession of the Mn and Fe moments in the ferrite sample, and the orbit of the precession is mapped out by introducing a variable time delay between the *rf* source and the x-ray bunch clock. Timing scans are presented in Fig. 3(c) (low temperature, 150 K) and in Fig. 3(d) (room temperature).

As expected, the oscillatory nature of the precession produces a sinusoidal trace, reflecting the time-varying projection

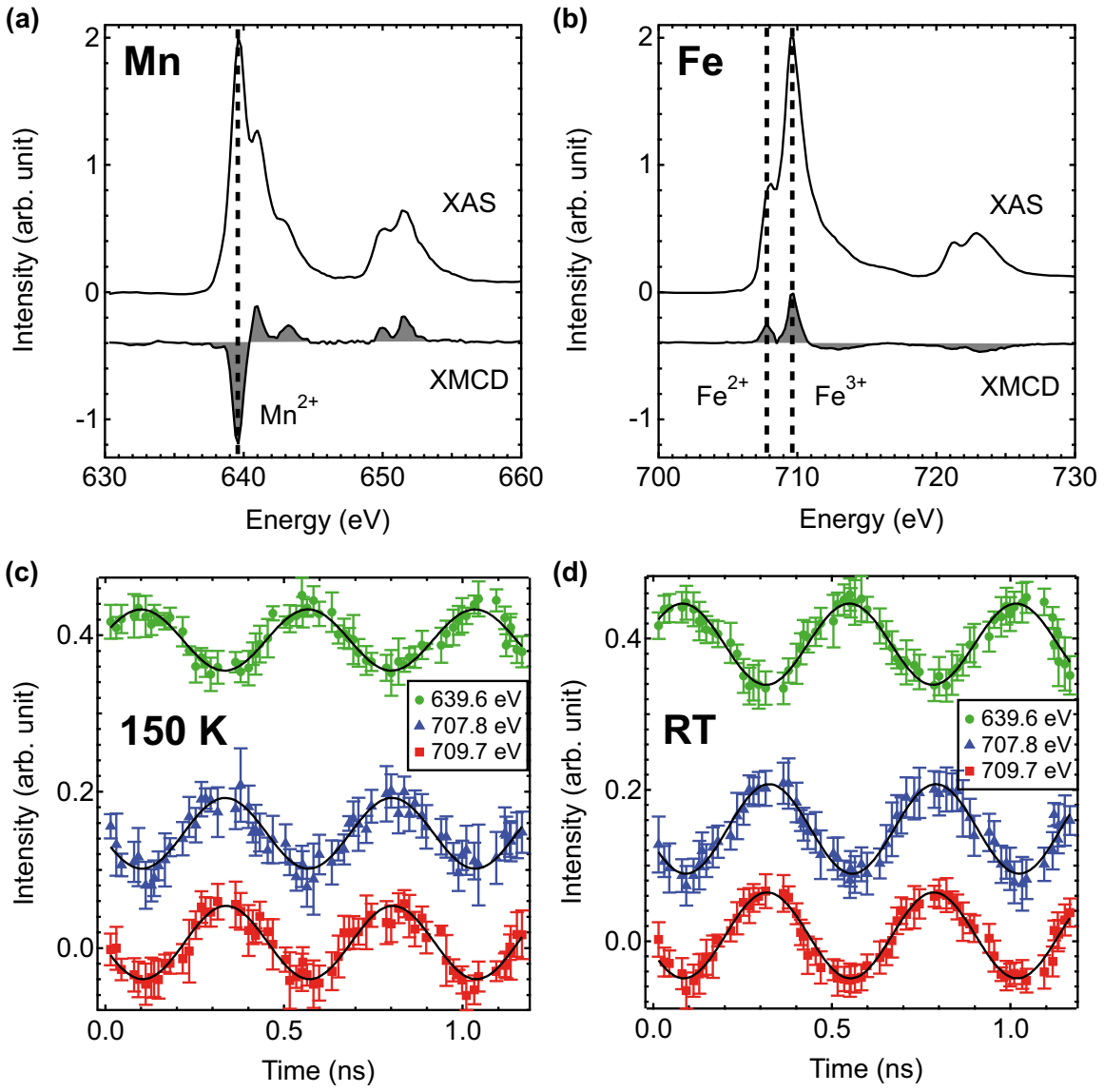

FIG. 3. (Color online) XAS and XMCD for Mn (a) and Fe (b) for a Mn-ferrite film grown on amorphous Si_3N_4 substrate. Dashed lines indicate the energies where the time delay scans are measured. Time delay scans showing the XMCD intensity as a function of time at 150 K (c) and room temperature (d) under continuous *rf* excitation of 2.1 GHz. The timing scans directly reveal predominantly antiphase precession between the Mn^{2+} (T_d) cations and $Fe^{2+,3+}$ (O_h) cations, although the Mn^{2+} (T_d) and Fe^{2+} (O_h) spins exhibit a subtle change in relative oscillation phase with temperature (see text).

of the precessing cation moments on the x-ray propagation direction. By fitting the delay traces, we extract the relative phase between the precession of the different cations. Taking the Mn^{2+} cations on T_d sites as our reference, the relative phase lag at 150 K is $181.2^\circ \pm 3.8^\circ$ for Fe^{2+} (O_h) and $183.3^\circ \pm 3.7^\circ$ for Fe^{3+} (O_h) corresponding to antiphase precession of the Fe cations relative to the Mn cation (estimated errors are 1σ values). The error in the extracted phases corresponds to a timing difference of ± 5 ps, well below the ~ 70 ps bunch width of the x rays used to sample the motion. At room temperature [Fig. 3(d)], the nearly antiphase precession between the Mn on T_d sites and Fe on O_h sites is again apparent. The observed phase lag relative to the Mn precession is unchanged for octahedrally coordinated Fe^{3+} ($182.0^\circ \pm 2.2^\circ$), while for Fe^{2+} on O_h sites the phase difference is $186.6^\circ \pm 2.2^\circ$.

IV. DISCUSSION

We have used high-resolution XAS and XMCD static measurements, combined with atomistic multiplet theory, to uniquely identify the spectral signature of Mn and Fe cations on different sublattices of the spinel structure. Combining such spectroscopy with an *in-situ* microwave excitation permits us to resolve the precession and spin alignment of the dissimilar cations in their local crystal field. The observation of precession under microwave excitation resolved to cations on specific lattice symmetries and distinct oxidation states establishes TR-XMCD as a technique that can address long-standing issues on relaxation processes in mixed-valence oxides. In many insulating oxides, the linewidth for microwave resonance varies considerably with temperature, reflecting a competition between the excitation frequency and temperature-dependent

relaxation processes, which can involve electron hopping between cations and symmetry sites [16].

In addition to the main ferrimagnetic ordering caused by the coupling between A and B sites, a coupling between similar cations at the octahedral sites, i.e., a BB coupling, has been suggested to cause a twisting of the magnetic order in some ferrites. The BB coupling can reach considerable values in some compounds where the octahedral sites are dominated by Mn, e.g., in $ZnMn_2O_4$ where the Mn^{3+}/Mn^{3+} interaction has been estimated to be $J \sim -19k$ [33] (where k is the Boltzmann constant). On the other hand, in compounds with dominant octahedral Fe occupancy the contribution is typically much smaller ($\sim 1k$) [34]. Although the BB coupling could affect ferrimagnetic ordering we expect the influence to be small due to the occupation of O_h sites by Fe cations.

In the present measurements, the Mn (T_d) and Fe (O_h) moments are seen to precess mostly antiphase with respect to each other, confirming that the cations on the T_d and O_h sites maintain their predominant antiferromagnetic alignment during *rf* excitation under the experimental conditions sampled thus far. Intriguingly, we observe that the phase difference between the the Mn^{2+} cations on T_d and the Fe^{2+} on O_h sites may increase *slightly* in going from 150 K to RT, although we note that the apparent difference may be due to statistical variations the current level of measurement noise. FMR measurements of similar Mn-ferrites show a linewidth increase of up to 60% at RT compared to 150 K [35,36], although linewidths in both those works and in the ferrite samples considered here are dominated by extrinsic (defect-mediated) mechanisms. Additional TR-XMCD measurements across a broader temperature range and with improved statistics may differentiate among the competing contributions to the temperature-dependent linewidth.

The clear identification of precession resolved to specific cations and crystalline sublattices establishes the capability to directly interrogate long-standing theories on ferromagnetic relaxation. Specific to the ferrite class, containing both mixed valence cations and dissimilar crystal symmetry sites, a more complete measurement of phase variation across a wide range of temperatures and at differing excitation frequencies should help distinguish between models of spin relaxation (e.g., frequency dependence for temperature-varying phase offsets and amplitude changes in valence exchange and slow relaxing impurity models [16]). We note that TR-XMCD under *rf* excitation can measure both the amplitude of the precession cone angle as well as the precession phase [37,38]. Such measurements may also reveal variations in the exchange stiffness between the T_d and O_h sites with temperature. Understanding and then controlling high frequency spin coupling in the spinel and other ferrite systems is essential to the design and realization of future generation microwave devices such as frequency selective limiters, phase shifters, filters, isolators, and circulators. Lastly, by directly examining cations or neutral species with different occupation of the d-state manifold, and hence different orbital moments, as a function of both temperature and frequency, phase-resolved XMCD may provide insights into the role of the orbital moment in loss processes necessary in magnetization dynamics [39,40].

ACKNOWLEDGMENTS

Use of the National Synchrotron Light Source (NSLS) at Brookhaven National Laboratory and the Advanced Photon Source (APS) at Argonne National Laboratory is supported by the U.S. Department of Energy (DOE), Office of Science, Office of Basic Energy Sciences, under Contract No. DE-AC02-98CH10886 (NSLS) and Contract No. DE-AC02-06CH11357 (APS).

[1] Z. Chen and V. G. Harris, J. Appl. Phys. **112**, 081101 (2012).
[2] U. Luders, M. Bibes, K. Bouzehouane, E. Jacquet, J. Contour, S. Fusil, J. Bobo, J. Fontcuberta, A. Barthelemy, and A. Fert, Appl. Phys. Lett. **88**, 082505 (2006).
[3] A. V. Ramos, M.-J. Guittet, J.-B. Moussy, R. Mattana, C. Deranlot, F. Petroff, and C. Gatel, Appl. Phys. Lett. **91**, 122107 (2007).
[4] S. Matzen, J.-B. Moussy, R. Mattana, K. Bouzehouane, C. Deranlot, and F. Petroff, Appl. Phys. Lett. **101**, 042409 (2012).
[5] P. van der Zaag, P. Bloemen, J. Gaines, R. Wolf, P. van der Heijden, R. van de Veerdonk, and W. de Jonge, J. Magn. Magn. Mater. **211**, 301 (2000).
[6] V. G. Harris, IEEE Trans. Magn. **48**, 1075 (2012).
[7] M. Pardavi-Horvath, J. Magn. Magn. Mater. **215-216**, 171 (2000).
[8] V. G. Harris, A. Geiler, Y. Chen, S. D. Yoon, M. Wu, A. Yang, Z. Chen, P. He, P. V. Parimi, X. Zuo, C. E. Patton, M. Abe, O. Acher, and C. Vittoria, J. Magn. Magn. Mater. **321**, 2035 (2009).
[9] G. v. d. Laan and I. Kirkman, J. Phys.: Condens. Matter **4**, 4189 (1992).
[10] E. Pellegrin, M. Hagelstein, S. Doyle, H. Moser, J. Fuchs, D. Vollath, S. Schuppler, M. James, S. Saxena, L. Niesen, O. Rogoianu, G. Sawatzky, C. Ferrero, M. Borowski, O. Tjernberg, and N. Brookes, Phys. Status Solidi B **215**, 797 (1999).
[11] J. A. Moyer, C. A. F. Vaz, D. A. Arena, D. Kumah, E. Negusse, and V. E. Henrich, Phys. Rev. B **84**, 054447 (2011).
[12] J. A. Moyer, D. P. Kumah, C. A. F. Vaz, D. A. Arena, and V. E. Henrich, Appl. Phys. Lett. **101**, 021907 (2012).
[13] V. L. Pool, C. Jolley, T. Douglas, E. A. Arenholz, and Y. U. Idzerda, J. Appl. Phys. **109**, 07B532 (2011).
[14] S. Suga and S. Imada, J. Electron Spectrosc. Relat. Phenom. **92**, 1 (1998).
[15] J. Takaobushi, M. Ishikawa, S. Ueda, E. Ikenaga, J.-J. Kim, M. Kobata, Y. Takeda, Y. Saitoh, M. Yabashi, Y. Nishino, D. Miwa, K. Tamasaku, T. Ishikawa, I. Satoh, H. Tanaka, K. Kobayashi, and T. Kawai, Phys. Rev. B **76**, 205108 (2007).
[16] M. Sparks, *Ferromagnetic Relaxation Theory* (McGraw-Hill, New York, 1965).
[17] J. M. Hastings and L. M. Corliss, Phys. Rev. **104**, 328 (1956).
[18] X. Zuo, A. Yang, S.-D. Yoon, J. A. Christodoulides, V. G. Harris, and C. Vittoria, Appl. Phys. Lett. **87**, 152505 (2005).
[19] A. Yang, Z. Chen, S. M. Islam, C. Vittoria, and V. G. Harris, J. Appl. Phys. **103**, 07E509 (2008).

[20] A. Yang, X. Zuo, C. Vittoria, and V. Harris, IEEE Trans. Magn. **42**, 2870 (2006).
[21] A. Yang, Z. Chen, A. L. Geiler, X. Zuo, D. Haskel, E. Kravtsov, C. Vittoria, and V. G. Harris, Appl. Phys. Lett. **93**, 052504 (2008).
[22] D. A. Arena, Y. Ding, E. Vescovo, S. Zohar, Y. Guan, and W. E. Bailey, Rev. Sci. Instrum. **80**, 083903 (2009).
[23] G. van der Laan and B. T. Thole, Phys. Rev. B **43**, 13401 (1991).
[24] E. Stavitski and F. M. F. de Groot, Micron **41**, 687 (2010).
[25] H. Ikeno, F. M. F. de Groot, E. Stavitski, and I. Tanaka, J. Phys.: Condens. Matter **21**, 104208 (2009).
[26] S. Matzen, J.-B. Moussy, R. Mattana, K. Bouzehouane, C. Deranlot, F. Petroff, J. C. Cezar, M.-A. Arrio, P. Sainctavit, C. Gatel, B. Warot-Fonrose, and Y. Zheng, Phys. Rev. B **83**, 184402 (2011).
[27] P. Kuiper, B. Searle, L.-C. Duda, R. Wolf, and P. van der Zaag, J. Electron Spectrosc. Relat. Phenom. **86**, 107 (1997).
[28] J.-S. Kang, G. Kim, H. J. Lee, D. H. Kim, H. S. Kim, J. H. Shim, S. Lee, H. G. Lee, J.-Y. Kim, B. H. Kim, and B. I. Min, Phys. Rev. B **77**, 035121 (2008).
[29] F. M. F. de Groot, J. Electron Spectrosc. Relat. Phenom. **67**, 529 (1994).
[30] E. Goering, M. Justen, J. Geissler, U. Rudiger, M. Rabe, G. Guntherodt, and G. Schutz, Appl. Phys. A: Mater. Sci. Process. **74**, 747 (2002).
[31] V. N. Antonov, B. N. Harmon, and A. N. Yaresko, Phys. Rev. B **67**, 024417 (2003).
[32] P. Warnicke, R. Knut, E. Wahlstrom, O. Karis, W. E. Bailey, and D. A. Arena, J. Appl. Phys. **113**, 033904 (2013).
[33] A. Broese van Groenou, P. Bongers, and A. Stuyts, Mater. Sci. Eng. **3**, 317 (1969).
[34] E. W. Gorter, J. Appl. Phys. **34**, 1253 (1963).
[35] A. G. Flores, V. Raposo, L. Torres, and J. Iniguez, J. Appl. Phys. **85**, 2293 (1999).
[36] P. E. Tannenwald, Phys. Rev. **100**, 1713 (1955).
[37] D. A. Arena, E. Vescovo, C. C. Kao, Y. Guan, and W. E. Bailey, Phys. Rev. B **74**, 064409 (2006).
[38] Y. Guan, W. Bailey, E. Vescovo, C. Kao, and D. Arena, J. Magn. Magn. Mater. **312**, 374 (2007).
[39] J. Kuneš and V. Kamberský, Phys. Rev. B **65**, 212411 (2002).
[40] K. Gilmore, Y. U. Idzerda, and M. D. Stiles, Phys. Rev. Lett. **99**, 027204 (2007).